Dynamic Stability and Reliability of Multi-Kilovolt GaN Monolithic Bidirectional HEMT

Yuan Qin[1#*], Yijin Guo[1#], Matthew Porter[1], Ming Xiao[3], Hehe Gong[1], Zineng Yang[1], Daniel Popa[4], Loizos Efthymiou[4], Kai Cheng[5], Zhiqin Chu[2], Han Wang[2], Florin Udrea[4,6*], Yuhao Zhang[2*]

[1]Center for Power Electronics Systems, Virginia Tech, Blacksburg, VA, USA

[2]Department of Electrical and Electronic Engineering, University of Hong Kong, Hong Kong, China

[3]Xidian University, Xi'an, China [4]Cambridge GaN Devices Ltd., Cambridge, UK

[5]Enkris Semiconductor Inc., Suzhou, China [6]University of Cambridge, Cambridge, UK

[#]These authors contributed equally to this work. [*]Corresponding authors: yuanqin@vt.edu, fu10000@cam.ac.uk, yuhzhang@hku.hk

***Abstract*—GaN monolithic bidirectional switch (MBDS) has the potential to enable revolutionary advances in AC power conversion. Despite the availability of industrial 650-V MBDS engineering samples, there have been very few reliability reports of GaN MBDS, and none has been performed up to kilovolt. Here we demonstrate a GaN enhancement-mode (E-mode) MBDS with high breakdown voltage (*BV*) over 3 kV in both polarities, and for the first time, study the dynamic stability and reliability of a GaN MBDS up to ±1.2 kV blocking voltage. The device deploys a dual p-GaN junction termination extension (D-JTE) design to achieve high *BV*. Pulse I-V, HTGB, and HTRB measurements were performed with an emphasis on the unique stress for bidirectional devices, including the reverse bias blocking and the impact of high-side gate. We find the dynamic on-resistance of the JTE-MBDS is sensitive to the low-side gate bias but insensitive to the high-side gate bias. Under the HTRB test, the MBDS shows larger shifts in on-resistance and threshold voltage under the reverse bias blocking compared to those under the forward bias blocking. Physical mechanisms are discussed and supported by TCAD simulations. Overall, our work suggests the importance of establishing a new framework for reliability evaluation of MBDS devices, which must account for the asymmetric trapping dynamics under bidirectional voltage blocking, as well as the impact of the second gate.**

Keywords—GaN, bidirectional switch, monolithic, stability, reliability, dynamic on-resistance, dynamic threshold voltage

I. Introduction

GaN power devices are key to advancing the electrical energy conversion towards a carbon-neutral society [1]. Their performance can be enhanced by architecture innovation [2]. A bidirectional switch (BDS), capable of bipolar voltage blocking in the off-state and bidirectional current conduction in the on-state, is a crucial component in AC power electronics applications. Monolithic BDS (MBDS) based on a single shared drift region can achieve a fourfold reduction in area compared to implementations using two discrete devices [3]. Recently, MBDS devices based on SiC MOSFETs [4], [5] and GaN HEMTs [6], [7], [8], [9], [10] have been reported. Lateral GaN HEMT-based MBDS uses a single drift region, enabling an increased advantage compared to SiC MBDS. Engineering samples of 650-V GaN MBDS are now available in industry [3]. However, there still lacks demonstrations of kilovolt-class GaN MBDS, although the advantage of MBDS compared to conventional BDS upscales with the voltage class. The other gap of GaN MBDS is stability and reliability. To date, there are only a few relevant reports [11], and most of them focusing on substrate bias management. Particularly, there still lacks bidirectional reliability studies at high voltage.

This work addresses these gaps by presenting the first stability and reliability data of a multi-kilovolt GaN MBDS at high bias up to ±1.2 kV. The device adopts a p-GaN-based D-JTE design that was recently proposed for GaN MBDS [12].

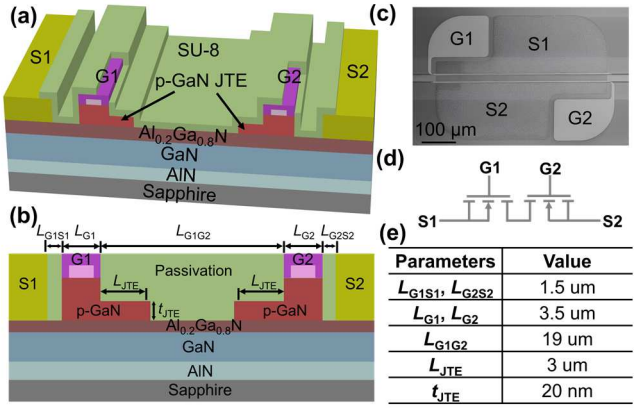

Parameters	Value
L_{G1S1}, L_{G2S2}	1.5 um
L_{G1}, L_{G2}	3.5 um
L_{G1G2}	19 um
L_{JTE}	3 um
t_{JTE}	20 nm

Fig. 1 (a) 3-D schematic of GaN MBDS with p-GaN D-JTE. (b) Cross-section view of the device with key geometric parameters. (c) Top-view SEM image and (d) equivalent circuit model of the device. (e) The list of key device parameters and values. Epi structure: AlN, 1.5 um GaN buffer, 200 nm GaN channel, 15 nm $Al_{0.2}Ga_{0.8}N$ barrier, 80 nm p-GaN cap layer ([Mg] ~ 2×10^{19} cm^{-3}).

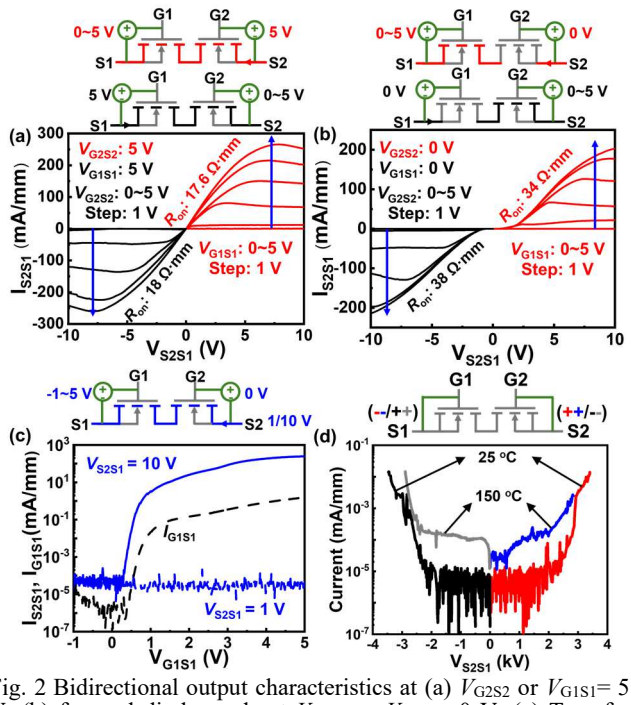

Fig. 2 Bidirectional output characteristics at (a) V_{G2S2} or V_{G1S1}= 5 V, (b) forward diode mode at V_{G2S2} or V_{G1S1}= 0 V. (c) Transfer characteristics I_{S2S1}-V_{G1S1} at V_{G2S2}= 0 V along with the gate leakage current. (d) Bipolar blocking characteristics of the GaN MBDS at 25 and 150 °C at V_{G2S2}= V_{G1S1} = 0 V. The corresponding test bias schemes are shown on top of each figure.

Benefitting from the more effective electric field (E-field) management than field plates, this JTE-MBDS achieves a breakdown voltage (*BV*) over 3 kV in both polarities. In this

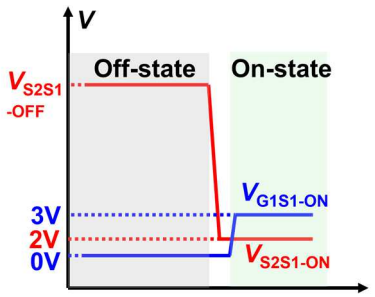

Fig. 3 Schematic of voltage waveform in the pulse I-V test for dynamic R_{on} using the Auriga system.

work, we characterize the high-temperature blocking capability, dynamic on-resistance, as well as the HTRB and HTGB reliabilities of such novel high-voltage GaN MBDS. An asymmetric parametric shift is observed in bidirectional (Bi-) HTRB test at source-to-source blocking bias (V_{S2S1}) of ±1.2 kV. The physics behind this asymmetry is also revealed.

II. Device Design and Static Characteristics

Fig. 1 shows the schematic of the GaN MBDS and some key device geometric parameters. Fig. 1(d) shows the equivalent circuit model of the fabricated device. The devices were fabricated on p-GaN gate HEMT platform on 100 mm sapphire substrate. Details of the epi structure and fabrication process are provided in [12].

Fig. 2 illustrates the bidirectional output, transfer characteristics, and bipolar blocking behavior of the fabricated GaN MBDS. The corresponding test bias schemes are shown on top of each figure. The R_{on} is calculated to be 17.6 Ω·mm and 18 Ω·mm in the 1st and 3rd quadrant, respectively. The specific R_{on} ($R_{on,sp}$) is then estimated to be 5.6 mΩ·cm^2 and 5.7 mΩ·cm^2 in the forward and reverse conduction mode, respectively. The R_{on} nearly doubles in forward diode mode (Fig. 2(b)) when V_{G2S2} or V_{G1S1}= 0 V. Fig. 2(c) presents the transfer curves of the device with G2 turned off (V_{G2S2}= 0 V) and the corresponding gate leakage current. No conduction current is observed until V_{S2S1} exceeds the turn-on voltage of G2. At V_{S2S1}= 10 V, G2 turns on, enabling current conduction between S1 and S2. The device is E-mode with V_{TH} = 0.6 V extracted at I_{S2S1}= 0.1 mA/mm. The gate leakage current is low at both V_{S2S1} = 1 V and 10 V, which can be further reduced by optimizing gate metal and the post annealing condition. As shown in Fig. 2(d), the GaN MBDS exhibits the bipolar blocking capability with BV over 3.4 kV at 25 °C and 2.8 kV at 150 °C. The test is performed under V_{G2S2} = V_{G1S1}= 0 V.

III. Pulse I-V Dynamic Test

On-wafer pulse I-V test was conducted to experimentally evaluate the dynamic performance of GaN MBDS. Fig. 3 shows the schematic of the voltage waveform during pulse I-V test. In on-state, $V_{G1S1\text{-}ON}$ = 3V, and $V_{S2S1\text{-}ON}$ = 2 V. While G1 switches between on and off, G2 remains on with a constant V_{G2S2} in the test. We then study the dependence of dynamic R_{on} on a few parameters, including V_{S2S1} and V_{G1S1} in the off-state ($V_{S2S1\text{-}OFF}$ and $V_{G1S1\text{-}OFF}$), as well as V_{G2S2}. Our test instrument (Auriga system) supports a maximum switching voltage of 1.2 kV, with the pulse width down to a few µs. As shown in Fig. 4(a), the widths of off- and on-state pulses are 2 µs and 5.5 µs, respectively. The device switched from a $V_{S2S1\text{-}OFF}$ of 1200 V to on-state voltage ($V_{S2S1\text{-}ON}$) of 3 V. In the pulse waveform, the current stabilizes within 1.5 µs after turn-on and the dynamic R_{on} is extracted 2 µs after turn-on.

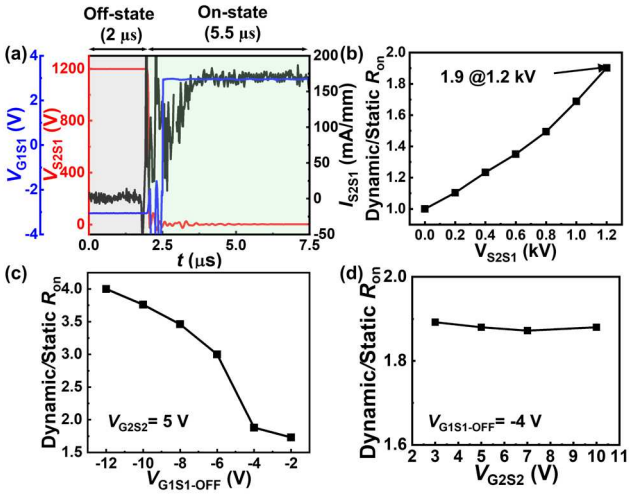

Fig. 4 (a) Dynamic switching waveforms at $V_{S2S1\text{-}OFF}$ = 1.2 kV. (b) The ratio between dynamic and static R_{on} versus V_{S2S1} of the GaN MBDS. $V_{G1S1\text{-}OFF}$ = 0V, $V_{G1S1\text{-}ON}$ = 3V, and $V_{S2S1\text{-}ON}$ = 2 V. (c) Dynamic/static R_{on} ratio as a function of $V_{G1S1\text{-}OFF}$ in the quiescent stress; $V_{S2S1\text{-}OFF}$ = 1.2 kV, $V_{S2S1\text{-}ON}$ = 2 V, $V_{G1S1\text{-}ON}$ = 3V, V_{G2S2} = 5 V. (d) Dynamic/static R_{on} ratio as a function of $V_{G2S2\text{-}ON}$; $V_{S2S1\text{-}OFF}$ = 1.2 kV, $V_{S2S1\text{-}ON}$ = 2 V, $V_{G1S1\text{-}ON}$ = 3V, and $V_{G1S1\text{-}OFF}$ = -4 V.

The GaN MBDS successfully switches up to 1.2 kV, with a dynamic R_{on} increase of approximately 1.9× (Fig. 4(b)). The shift in dynamic R_{on} is investigated by varying the $V_{G1S1\text{-}OFF}$ in the quiescent stress and adjusting V_{G2S2} during the pulse I-V test, as shown in Fig. 4(c)-(d). The $V_{G1S1\text{-}OFF}$ significantly impacts dynamic R_{on}, increasing it by approximately 4× at $V_{G1S1\text{-}OFF}$ = -12 V. In contrast, V_{G2S2} has minimal influence on dynamic R_{on}. The physics will be discussed in Section V.

IV. Long Term Reliability Test

The longer-term reliability tests were performed on the GaN MBDS under various stress conditions. As shown in Fig. 5, G1 is subjected to HTGB test at V_{G1S1}= ±6 V, while the device is bidirectionally stressed at V_{S2S1}= ±1.2 kV for the Bi-HTRB test, both conducted at T= 150 °C. In both tests, stress durations increase from 1 s to 1000 s, with transfer and output

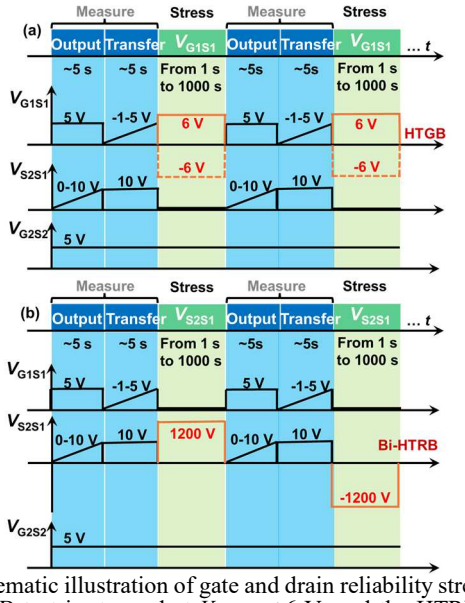

Fig. 5 Schematic illustration of gate and drain reliability stress tests. The HTGB test is stressed at V_{G1S1}= ±6 V, and the HTRB test is bidirectionally stressed at V_{S2S1}=±1.2 kV, both at T= 150 °C. V_{G1S1} for output sweep is 5 V, and V_{S2S1} for transfer characteristics sweep is 10 V. V_{G2S2} remains fixed and continuously biased at 5V.

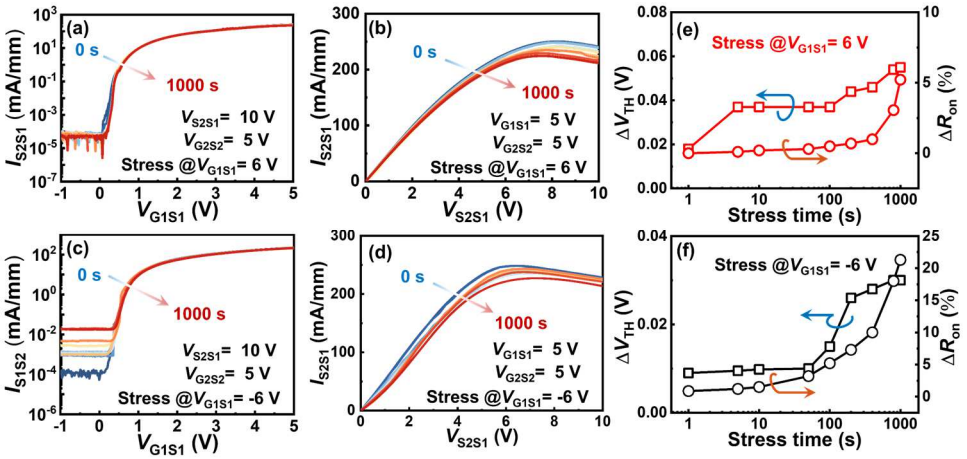

Fig. 6 Evolution of (a) transfer and (b) output I-V characteristics in the HTGB test at V_{G1S1}=6 V. Evolution of (c) transfer and (d) output I-V characteristics in the HTGB test at V_{G1S1}=-6 V. Evolution of ΔV_{TH} and ΔR_{on} as a function of stress time during HTGB test at (c) V_{G1S1}=6 V and (f) V_{G1S1}=-6 V. All tests were performed at 150 °C.

characteristics measured intermittently after each stress cycle. During the reliability test, V_{G2S2} remains fixed at 5 V.

Fig. 6 shows the evolution of transfer and output characteristics, along with the shifts in V_{TH} and R_{on} shift under HTGB test. Under both V_{G1S1}= 6 V and -6 V stress, negligible shifts in V_{TH} are observed after a stress of 1000 s. R_{on} increases more under stress of V_{G1S1}= -6 V with approximately 22 %. An increased off-state leakage current is also observed under HTGB stress at V_{G1S1}= -6 V, potentially attributed to the trap-assisted tunneling of the p-GaN/AlGaN/GaN p-i-n junction.

During the Bi-HTRB test, V_{S2S1} is first stressed at 1.2 kV, followed by the measurement of output and transfer characteristics. In the next cycle, V_{S2S1} is stressed at -1.2 kV, and output and transfer curves are recorded. This process is repeated until the stress time in a cycle reaches 1000 s. This profile mimics the practical converter application in which the BDS blocks bipolar biases alternatively. Fig. 7 presents the transfer and output characteristics evolution, along with the V_{TH} and R_{on} shift during the Bi-HTRB test at V_{S2S1}= ±1.2 kV. Under 1.2 kV stress, the V_{TH} experiences a slight negative shift. In contrast, V_{TH} shifts positively by 0.26 V under -1.2 kV stress. The R_{on} increases in both stress conditions with ΔR_{on} of 32% and 40% under 1.2 kV and -1.2 kV HTRB stress, respectively. These asymmetric parameters shift in Bi-HTRB test is attributed to differences in E-field distribution under V_{S2S1}= ±1.2 kV, which alters trapping dynamics. The underlying mechanisms will be discussed in the next section.

V. Physical Mechanism

This section explores the physical mechanism of the substantial dynamic R_{on} increase in the pulse I-V test with negative off-state V_{G1S1} as well as the asymmetric shifts in V_{TH} and R_{on} observed in Bi-HTRB tests at V_{S2S1}= ±1.2 kV. Fig. 8 depicts carrier dynamics in the off-state with V_{S2S1}= ±1.2 kV, with G1 negatively biased. Fig. 9 shows the simulated E-field and hole concentration contours inside the device at V_{S2S1}= ±1.2 kV with V_{G1S1} = -4 V and V_{G2S2} = 5 V.

Under V_{S2S1}= 1.2 kV, high E-field is located at the G1 and its connected JTE1 (Fig. 9(a)). Such high field can induce electron trapping at the AlGaN surface and within passivation layer [13]. When G1 is more negatively biased, electron injection from G1 enhances trapping (Fig. 8(a)). This mechanism explains the increased dynamic R_{on} observed when $V_{G1S1\text{-}OFF}$ is more negatively biased in the pulse I-V test, as well as the R_{on} shift in the HTRB test.

Note that the V_{TH} exhibits minimal shift under 1.2 kV HTRB test. This can be explained by the hole depletion in JTE1 (Fig. 9(b)), which leaves negatively charged acceptors in JTE. As a result, the electrons injected from G1 are repelled away from the p-GaN region (see Fig. 8(a)).

Under V_{S2S1}= -1.2 kV and V_{G2S2}= 5 V, the device pinches off near the G1 and JTE1, resulting in a much higher E-field and stronger depletion in the p-GaN there. Fig. 9(c) and (d) reveals a peak E-field of 3.5 MV/cm crowded at G1 gate edge

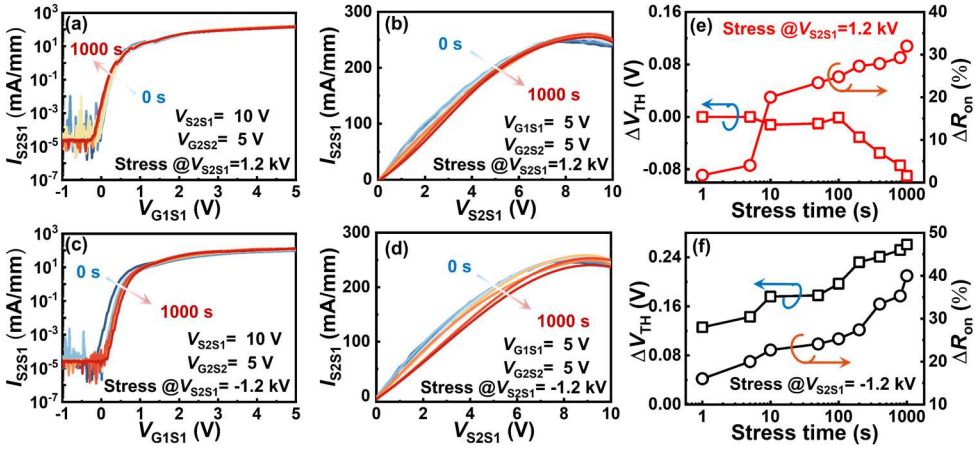

Fig. 7 Evolution of (a) transfer and (b) output I-V characteristics during HTRB test at V_{S2S1}=1.2 kV. Evolution of (c) transfer and (d) output I-V characteristics during HTRB test at V_{S2S1}=-1.2 kV. Evolution of ΔV_{TH} and ΔR_{on} as a function of stress time during HTRB test at (e) V_{S2S1}=1.2 kV and (f) V_{S2S1}=-1.2 kV. All tests were conducted at 150 °C.

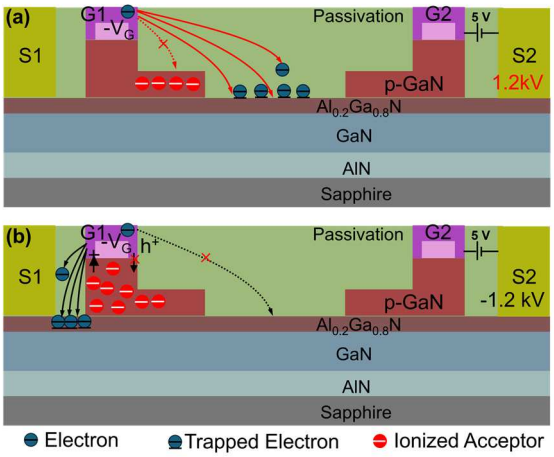

Fig. 8 Illustration of carrier dynamics under (a) V_{S2S1}=1.2 kV stress and (b) V_{S2S1}= -1.2 kV stress, both with negative V_{G1S1}.

and a nearly full depletion of p-GaN under G1 and JTE1. The full depletion of p-GaN, in contrast to the minimal p-GaN depletion under 1.2 kV stress, explains the large V_{TH} shift only present under -1.2 kV stress. This is because Schottky-type p-GaN gate functions as a back-to-back configuration of a p-GaN Schottky junction and a p-GaN/AlGaN/GaN p-i-n junction. Right after turn-on, the p-GaN Schottky junction becomes reversely biased, impeding efficient hole supply (Fig. 8(b)) [14]. Consequently, the remaining negatively charged ionized acceptors induce a positive V_{TH} shift.

Meanwhile, under the -1.2 kV stress, the high E-field in the region between S1 and G1 promotes electron trapping at the AlGaN surface and within the passivation layer (Fig. 8(b)), further exacerbating the V_{TH} shift. The larger R_{on} shift is also observed in the -1.2 kV HTRB test, primarily due to two factors: (1) the positive shift in V_{TH} and (2) intensified electron trapping effect in the S1-G1 access region due to higher E-field. In general, due to the stronger E-field crowding and full p-GaN depletion, parametric shifts are more serious under -1.2 kV stress compared to under 1.2 kV stress.

VI. Conslusion

This work presents the dynamic stability and reliability studies of a >3 kV GaN E-mode MBDS under a bipolar bias stress up to ±1.2 kV. This is the first reliability studies of GaN MBDS under kilovolt operation. In general, despite the symmetric static characteristics, the dynamic R_{ON} and device parametric shifts under HTRB and HTGB all exhibit a certain level of asymmetry in terms of the polarities of stresses and the impacts of the two gates. This is attributable to the subtle electrostatic differences when the device is subject to bipolar bias stresses and the induced difference in carrier trapping. The device parametric shift is found to be more serious under the reverse blocking stress compared to the forward blocking stress. These results suggest the reliability of GaN MBDS cannot be sufficiently evaluated under the conventional framework for unidirectional GaN HEMT and demand a more comprehensive framework involving bidirectional stresses.

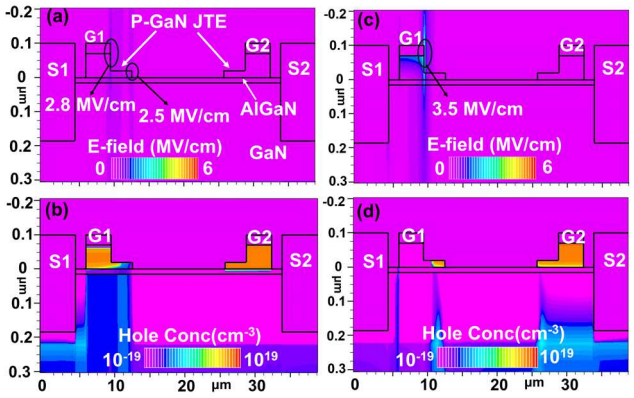

Fig. 9 Simulated (a) E-field distribution and (b) contour of hole concentration in the GaN MBDS under V_{S2S1}=1.2 kV. Simulated (c) E-field distribution and (d) contour of hole concentration under V_{S2S1}=-1.2 kV. V_{G1S1} = -4 V and V_{G2S2} = 5 V.

Acknowledgment

This study is supported in part by the CPES Industry Consortium and in part by the National Science Foundation under grants ECCS-2424859 and ECCS-2230412.

References

[1] Y. Zhang, D. Dong, Q. Li, R. Zhang, F. Udrea, and H. Wang, "Wide-bandgap semiconductors and power electronics as pathways to carbon neutrality," *Nature Review Electrical Engineering*, vol. 2, no. 3, 155-172, Jan. 2025.

[2] Y. Zhang, F. Udrea, and H. Wang, "Multidimensional device architectures for efficient power electronics," *Nature Electronics*, vol. 5, no. 11, Art. no. 11, Nov. 2022.

[3] J. Huber and J. W. Kolar, "Monolithic Bidirectional Power Transistors," *IEEE Power Electronics Magazine*, vol. 10, no. 1, pp. 28–38, Mar. 2023.

[4] K. Han *et al.*, "Monolithic 4-Terminal 1.2 kV/20 A 4H-SiC Bi-Directional Field Effect Transistor (BiDFET) with Integrated JBS Diodes," in *2020 32nd International Symposium on Power Semiconductor Devices and ICs (ISPSD)*, Vienna, Austria: IEEE, Sep. 2020, pp. 242–245.

[5] S. Y. Jang, S. A. Mancini, and W. Sung, "600 V 4H-SiC Lateral Bi-Directional JBS Diode Integrated MOSFET (L-BiD-JBSFET)," in *2024 36th International Symposium on Power Semiconductor Devices and ICs (ISPSD)*, Bremen, Germany: IEEE, Jun. 2024, pp. 335–338.

[6] T. Morita *et al.*, "650 V 3.1 mΩ·cm^2 GaN-based monolithic bidirectional switch using normally-off gate injection transistor," in *2007 IEEE International Electron Devices Meeting*, Washington, DC, USA: IEEE, 2007, pp. 865–868.

[7] C. Kuring, O. Hilt, J. Bocker, M. Wolf, S. Dieckerhoff, and J. Wurfl, "Novel monolithically integrated bidirectional GaN HEMT," in *2018 IEEE Energy Conversion Congress and Exposition (ECCE)*, Portland, OR, USA: IEEE, Sep. 2018, pp. 876–883.

[8] G. Gupta *et al.*, "Innovations in GaN Four Quadrant Switch technology," in *2023 IEEE 10th Workshop on Wide Bandgap Power Devices & Applications (WiPDA)*, Charlotte, NC, USA: IEEE, Dec. 2023, pp. 1–4.

[9] M. T. Alam, J. Chen, R. Bai, S. S. Pasayat, and C. Gupta, "High-Voltage (>1.2 kV) AlGaN/GaN Monolithic Bidirectional HEMTs With Low On-Resistance (2.54 mΩ·cm^2)," *IEEE Transactions on Electron Devices*, vol. 71, no. 1, pp. 733–738, Jan. 2024.

[10] G. Baratella *et al.*, "Monolithic 650-V Dual-Gate p-GaN Bidirectional Switch," *IEEE Transactions on Electron Devices*, vol. 71, no. 11, pp. 6904–6909, Nov. 2024.

[11] X. Geng *et al.*, "Experimental Investigation of GaN-on-AlN/SiC Transistors With Regard to Monolithic Integration," *IEEE Transactions on Power Electronics*, vol. 39, no. 10, pp. 12615–12624, Oct. 2024.

[12] Y. Guo *et al.*, "Enhancement-mode GaN Monolithic Bidirectional Switch with Breakdown Voltage over 3.3 kV," *IEEE Electron Device Letters*, pp. 1–1, 2025.

[13] Q. Song *et al.*, "Stability Improvement of GaN Power HEMT by a Multifunctional Monolithic Protection Circuit," *IEEE Transactions on Power Electronics*, vol. 40, no. 4, pp. 5212–5222, Apr. 2025.

[14] B. Wang, Q. Song, and Y. Zhang, "Gate Switching Lifetime of P-Gate GaN HEMT: Circuit Characterization and Generalized Model," *IEEE Transactions on Power Electronics*, vol. 39, no. 12, pp. 16091–16102, Dec. 2024.